

From 2D Images to 3D Model: Weakly Supervised Multi-View Face Reconstruction with Deep Fusion

Weiguang Zhao^{a,1}, Chaolong Yang^{a,1}, Jianan Ye^{b,1}, Rui Zhang^{c,*}, Yuyao Yan^d, Xi Yang^d, Bin Dong^e, Amir Hussain^f, Kaizhu Huang^{g,*}

^a*Department of Computer Science, University of Liverpool, Liverpool L69 7ZX, UK.*

^b*Department of Electrical Engineering and Electronics, University of Liverpool, Liverpool L69 7ZX, UK.*

^c*Department of Foundational Mathematics, Xi'an Jiaotong-Liverpool University, Suzhou, 215123, China.*

^d*Department of Electrical and Electronic Engineering, Xi'an Jiaotong-Liverpool University, Suzhou, 215123, China.*

^e*Ricoh Software Research Center (Beijing) Co., Ltd., Beijing 100000, China.*

^f*School of Computing, Edinburgh Napier University, Edinburgh, EH11 4BN, UK.*

^g*Data Science Research Center, Duke Kunshan University, Kunshan, 215316, China.*

Abstract

While weakly supervised multi-view face reconstruction (MVR) is garnering increased attention, one critical issue still remains open: how to effectively fuse multiple image information to reconstruct high-precision 3D models. In this regard, we propose a novel model called Deep Fusion MVR (DF-MVR) and design a multi-view encoding to single decoding framework with skip connections, able to extract, integrate, and compensate deep features with attention from multi-view images. Furthermore, we adopt the involution kernel to

*Corresponding author

Email addresses: Weiguang.Zhao@liverpool.ac.uk (Weiguang Zhao), Chaolong.Yang@liverpool.ac.uk (Chaolong Yang), J.Ye13@liverpool.ac.uk (Jianan Ye), Rui.Zhang02@xjtlu.edu.cn (Rui Zhang), Yuyao.Yan@xjtlu.edu.cn (Yuyao Yan), Xi.Yang01@xjtlu.edu.cn (Xi Yang), Bin.Dong@srcb.ricoh.com (Bin Dong), A.Hussain@napier.ac.uk (Amir Hussain), Kaizhu.Huang@dukekunshan.edu.cn (Kaizhu Huang)

¹Equal contribution

enrich deep fusion features with channel features. In addition, we develop the face parse network to learn, identify, and emphasize the critical common face area within multi-view images. Experiments on Pixel-Face and Bosphorus datasets indicate the superiority of our model. Without 3D annotation, DF-MVR achieves 5.2% and 3.0% RMSE improvement over the existing weakly supervised MVRs respectively on Pixel-Face and Bosphorus dataset. Code will be available publicly at https://github.com/weiguangzhao/DF_MVR.

Keywords: Face reconstruction, Feature fusion, Multi-view, 3DMM.

1. Introduction

Reconstructing 3D shapes of human faces from 2D images is a challenging yet essential task for numerous applications [1, 2, 3] such as virtual reality, augmented reality, and facial animations. The 3D Morphable Model (3DMM) [4] is the pioneer in converting the 3D face model to a parameter representation. Recently, adopting convolutional neural networks (CNN) to extract 2D image information to predict 3DMM coefficients has become the mainstream method of face reconstruction. Supervised CNN-based methods [5, 6, 7] demand a substantial quantity of 3D face meshes or point clouds [8, 9] corresponding to 2D images as ground-truth, which are time and/or manpower consuming.

To alleviate the need for 3D face meshes or point clouds data, recent efforts have shifted to weakly supervised and self-supervised methods [10, 11, 12, 13, 14, 15]. Most of these methods use landmarks and differentiable rendering for training. However, these methods only exploit one single image for reconstruction, which usually fail to estimate facial depth appropriately.

For instance, they cannot fully explain the geometric difference of facial features, such as the height of the mouth and eye sockets. Such limitation can however be resolved by the geometric constraints contained in a few face images of different views, or multi-view images. Surprisingly, only a handful of studies have been made on weakly supervised multi-view 3D face reconstruction tasks [16, 17, 18]. These methods are unfortunately limited because they simply concatenate multi-view image features and do not consider deep fusion of multi-view images features, nor do they pay attention to critical areas (e.g. eye, brow, nose, and mouth) which may impact the reconstruction quality the most.

To cope with these drawbacks, we propose a novel end-to-end weakly supervised multi-view 3D face reconstruction network which learns to fuse deep representations and identify critical areas. First, as multi-view images all represent the same face, we develop an encoding-decoding network (Tri-Unet) with attention to extract features and deeply fuse them into one feature map. As shown in Fig. 3, multiple encoders are used to extract features from multi-view images, and one single decoder is engaged to fuse these features in deep. In order to compensate for the possible loss caused by sampling, skip connections with attention are introduced. Second, we bridge the involution [19] to extract more flexibly channel features than traditional convolution, which is typically utilized in face reconstruction networks. Finally, we develop a multi-view face parse network to learn, identify, and emphasize the critical common face areas. The face parse network is able to learn the face mask which not only acts as input features to help Tri-Unet encode/decode common area of multi-view images for better deep fusion, but also plays the role

of a weight map to calculate the pixelwise photometric loss between rendered images and original images. Finally, combining pixelwise photometric loss, mask loss, and landmark loss, we design a novel weakly supervised training framework that is able to fuse deep features comprehensively and pay attention to critical face features specially.

The contributions of our work are as follows:

- We propose a novel weakly supervised multi-view face reconstruction framework incorporating Tri-Unet and involution. Tri-Unet, enhanced with attention, is designed to extract multi-view features and fuse them into a unified feature map. Furthermore, the involution is adopted to enrich deep fusion features with the channel feature. To our best knowledge, we make the first attempt to bridge the involution to 3D face reconstruction.
- We develop face mask mechanism to facilitate feature fusion and facial reconstruction. It identifies common areas of multi-view images in the fusion progress. On the other hand, it acts as weight map to encourage the 3D face reconstruction network to pay more attention to critical areas (e.g. eye, brow, nose, and mouth).
- On the empirical side, our novel framework achieves 5.2% and 3.0% RMSE improvement over the existing weakly supervised MVRs respectively on Pixel-Face and Bosphorus dataset without 3D annotation.

2. Related Work

2.1. 3D Morphable Model

3D Morphable Model (3DMM) is a statistical model of 3D facial shape and texture which performs principal component analysis (PCA) on the face mesh training set [4, 20]. Subsequently, the Basel Face Model (BFM) [21] is released as a generative 3D shape and texture model and demonstrates its application to several face recognition tasks. LSFM [22] has further expanded 3DMM to build models for specific ages, genders or ethnic groups. The current multi-view reconstruction methods mostly use BFM. For a fair comparison, we also exploit BFM to represent 3D faces in our model.

2.2. Mask in 3D face reconstruction

Currently, most 3D face reconstruction methods utilize the skin mask [23] to obtain the pixel positions of the face, thereby eliminating background interference. Deep3DFace [16] proposes a robust, skinaware photometric loss to reduce the effects of occlusion. FOCUS-MP [15] develops skin mask to attain the highly robust face reconstruction network. While there are some pioneer works probing face mask in the face reconstruction, THFNet [24] utilizes face mask to peel off eyes and brows to focus on the texture of the face skin. GFPMG [25] adopts the face parsing network to remove the occlusion and restore the face image to achieve the full 3D face. Most of these methods utilize the face parsing network for the occlusion localization in the task of single-view 3D face reconstruction. Different from these approaches, our method develops the face parsing network to promote multi-view feature fusion and increases the reconstruction weight of critical areas.

2.3. Single-view 3D face reconstruction Methods

Most single-view face reconstruction methods take CNN as the deep learning network to predict 3DMM coefficients [26, 27, 28]. For example, 3DFFA [26] deploys CNN to predict 3DMM coefficients and achieves encouraging results. Rrd3d [27] designs a robust method, based on CNN and ResNet101 [29], to regress 3DMM shape and texture coefficients directly from an input photo without annotation of landmarks. UH-E2FAR [30] concatenates the last two pooling layers of CNN to create a Fusion CNN branch for predicting the expression base individually. It also generates synthetic rendered face images with predicted 3D scans. PerspNet [28] proposes to reconstruct 3D face shape in canonical space and learn the correspondence between 2D pixels and 3D points. However, these methods all require 3D mesh files as ground-truth, which greatly hinders their practical applications due to the shortfall of available annotated training data containing 3D shapes.

To cope with this issue, recent research focus has been put on weakly supervised and self-supervised methods. Mofa [10] and UT3DMMR [31] propose a model that can be trained without 3D labels by adopting differentiable rendering for calculating the pixel difference between the rendered image and the original image. SFSNet [32] designs an end-to-end learning framework for accurately decomposing an unconstrained human face image into shape, reflectance and illuminance. THFNet [24] uses a similar method to predict 3D shapes while further adding GAN to generate more detailed texture information.

2.4. Multi-view 3D face reconstruction Methods

Multi-view methods [5, 33, 34, 35] can provide more geometric constraints and structural information than single-view methods. DRFAR [5] proposes to use Recurrent Neural Network (RNN) to fuse identity-related features extracted from deep convolutional neural network (DCNN) to produce more discriminative reconstructions, but their approach does not exploit multi-view geometric constraints. MVFNet [35] adds multi-view geometric constraints and introduces the optical flow loss to improve the reconstruction accuracy. In the feature extraction of multiple images, they only concatenate the deep features. All these methods require ground-truth of 3DMM, which is hardly available practically.

Surprisingly, there are few multi-view 3D face reconstruction methods based on weakly supervised machine learning in the literature. Deep3DFace [16] designs two CNN models for predicting 3DMM coefficients and scoring each image. The image with high confidence is used to regress shape coefficients, and the rest images will be used to regress coefficients such as expression and texture. MGCNet [17] adopts the concept of geometry consistency to design pixel and depth consistency loss. They establish dense pixel correspondences across multi-view input images and introduce the covisible maps to account for the self-occlusion. Furthermore, HRN [36], to be precise, is a semi-supervised approach that utilizes the complete 3D ground-truth to generate deformation and displacement map for training. However, these methods pay less attention to the local features of the face and the feature fusion of multiple images. In contrast, our method not only designs the Tri-Unet and involution framework to fuse multi-view features, but also employs

the mask mechanism to promote multi-view feature fusion and focus on the reconstruction of critical areas.

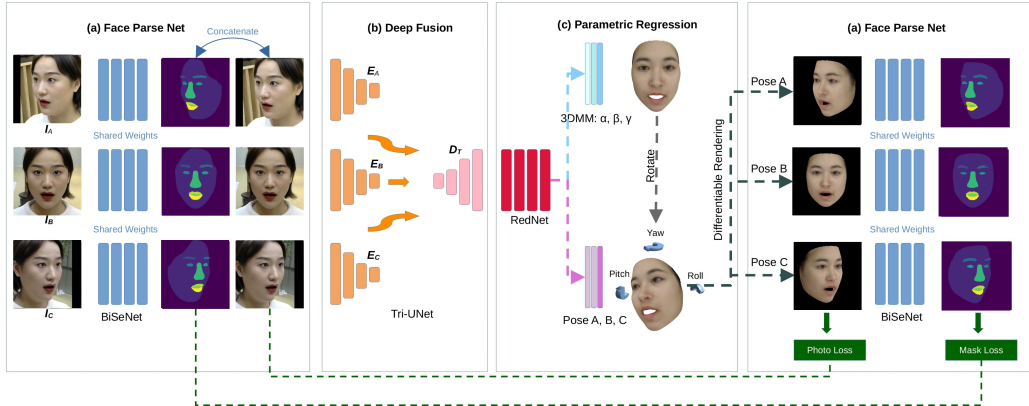


Figure 1: Overview of DF-MVR

3. Main Methodology

3.1. Overview

We first provide an overview of our proposed framework, which is shown in Fig. 1. We decide to exploit three multi-view images of a subject for generating a corresponding 3D face and introduce the *face parse network* (a) to process these three images separately to generate unified standard face masks. An *encoding-decoding network* (b) is designed to fuse the features of multi-view images in deep by sharing a decoder with an attention mechanism to obtain information from the encoder. Moreover, RedNet [19] with involution is used as *parametric regression* (c) to regress 3DMM and pose coefficients. The reconstructed 3D face is reoriented utilizing the pose coefficients and then rendered back to 2D. The photo loss between the re-rendered 2D image

and the input image at the target view is calculated while the masks are exploited as the weight map to enhance the back propagation of the facial features. In this section, we will provide details on each component as below.

3.2. Face Parse Net

We introduce the face parse network based on BiSeNet [37] to perform preliminary analysis of the input image and identify the elements of the image. The generated face mask has only one layer of channel. For example, if the size of the input image is $224 \times 224 \times 3$, the size of the face mask will be $224 \times 224 \times 1$. In order to better highlight the face, excessive elements of face masks such as hair and neck, will be removed, and the following parts will be kept: background, face skin, left brow, right brow, left eye, right eye, nose, mouth, upper lip, and lower lip. The reserved parts are marked with different numbers in order to distinguish facial features. As shown in Fig. 2, one-hot encoding is leveraged to assign the label for these parts. On one hand, the face masks are concatenated with the original images to help the network understand the common area of the multi-view image. On the other hand, the face masks serve as weight map to calculate the photo loss and mask loss for training.

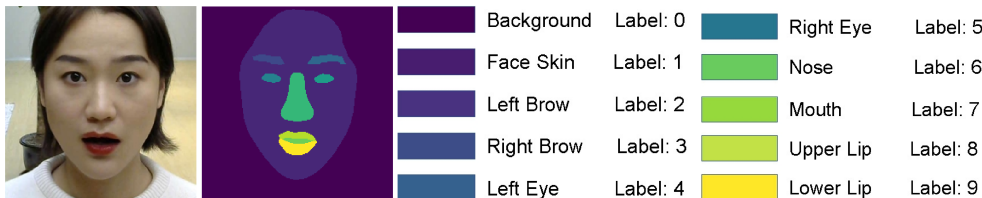


Figure 2: Face Mask Annotation.

3.3. Deep Fusion

The existing multi-view face reconstruction networks all deploy CNN or VGG as the feature extractor. These networks concatenate the multi-graph features in the fully connected layer, which cannot perform feature interaction well. In addition, the previous networks mostly adopt shared weights or one backbone to process multi-view images, making it difficult for the network to pay attention to the unique information of each view. Differently, we design a novel feature fusion network, Tri-UNet, to extract features of multi-view images inspired by attention Unet [38].

We denote the three-view input images as \mathbf{I}_A , \mathbf{I}_B , and \mathbf{I}_C , representing the three perspectives of left, front and right. Since the information and focus of each view are different, we set up three encoders to extract the features from three views respectively. Corresponding to the input images, these three encoders are represented by \mathbf{E}_A , \mathbf{E}_B , and \mathbf{E}_C . The weights of the three encoders are not shared. Encoders are mainly composed of double convolution and maximum pooling. At the end of encoders, the deep features of \mathbf{I}_A , \mathbf{I}_B , \mathbf{I}_C will be concatenated as \mathbf{F}_D . Considering that \mathbf{I}_A , \mathbf{I}_B , and \mathbf{I}_C actually describe the same object, we only set up a shared decoder for better fusing features as well as emphasizing the common features. The decoder is mainly composed of ConvTranspose, convolution, concatenate and skip connection. We adopt the attention mechanism [39, 40, 41] to extract the feature \mathbf{F}_A , \mathbf{F}_B , and \mathbf{F}_C from \mathbf{E}_A , \mathbf{E}_B , and \mathbf{E}_C to enrich the information in the \mathbf{F}_D decoding process. Finally, the fusion feature size we retain is $224 \times 224 \times 64$, in the case where the image size is $224 \times 224 \times 3$.

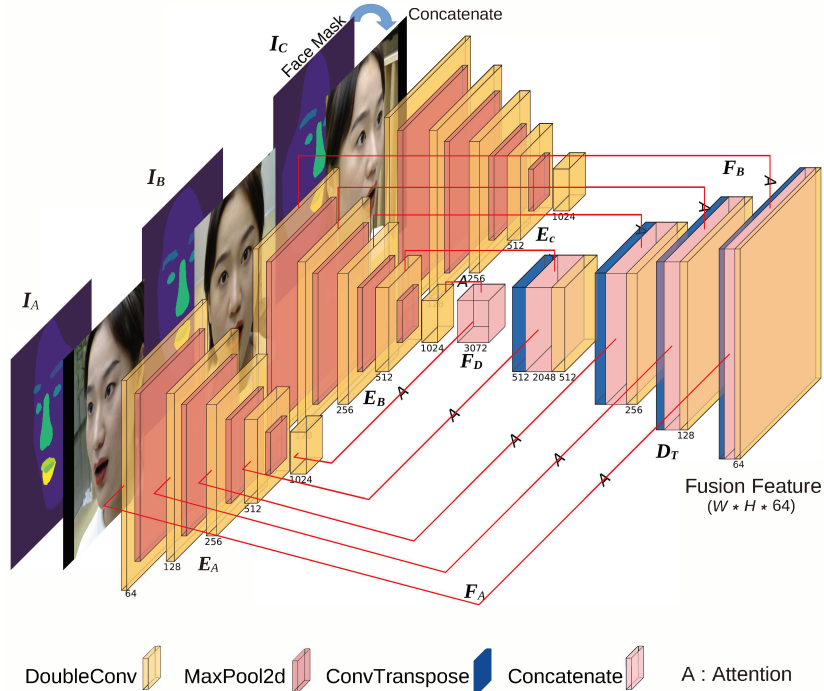


Figure 3: Tri-UNet. For conciseness, we do not draw the skip connection of the \mathbf{E}_C , which is similar to the \mathbf{E}_A .

3.4. Parametric Regression

We adopt RedNet50 to process the fusion features and regress parameters. RedNet replaces traditional convolution with involution on the ResNet architecture. The inter-channel redundancy within the convolution filter stands out in many deep neural networks, casting the flexibility of convolution kernels w.r.t. different channels into doubt. Compared with traditional convolution, involution is spatial-specific and able to obtain features on the channel. Therefore, we choose RedNet to perform parameter regression, and ablation experiments also verify its effectiveness.

3DMM Parameters regressed in this work include identification, expres-

sion, and texture parameters. The 3D face shape \mathbf{S} and the texture \mathbf{T} can be represented as:

$$\begin{aligned}\mathbf{S} &= \mathbf{S}(\boldsymbol{\alpha}, \boldsymbol{\beta}) = \bar{\mathbf{S}} + \mathbf{B}_{id}\boldsymbol{\alpha} + \mathbf{B}_{exp}\boldsymbol{\beta}, \\ \mathbf{T} &= \mathbf{T}(\boldsymbol{\gamma}) = \bar{\mathbf{T}} + \mathbf{B}_t\boldsymbol{\gamma},\end{aligned}\tag{1}$$

where $\bar{\mathbf{S}}$ and $\bar{\mathbf{T}}$ are the average face shape and texture. \mathbf{B}_{id} , \mathbf{B}_{exp} , \mathbf{B}_t are the PCA bases of identity, expression, and texture respectively. $\boldsymbol{\alpha}$, $\boldsymbol{\beta}$, and $\boldsymbol{\gamma}$ are the parameter vectors that the network needs to regress ($\boldsymbol{\alpha}, \boldsymbol{\beta} \in R^{80}$ and $\boldsymbol{\gamma} \in R^{64}$). By adjusting these three vectors, the shape, expression and texture of the 3D face can be changed. In order to compare with MGCNet [17] and Deep3DFace [16] fairly, we use the same face model. BFM [21] is adopted for $\bar{\mathbf{S}}, \mathbf{B}_{id}, \bar{\mathbf{T}}$, and \mathbf{B}_t . \mathbf{B}_{exp} [7] is built based on Facewarehouse [42].

Pose Parameters are used to adjust the angle and position of the 3D face in the camera coordinate system. We exploit the differentiable perspective rendering [43] to render the 3D face back to 2D. When the camera coordinates are fixed, we could change the size and angle of the rendered 2D face by adjusting the position of the 3D face in the camera coordinate system. Meanwhile, the position of the 3D face in the camera coordinate system can be determined by predicting the rotation angle and translation in each axis. In order to enhance the geometric constraints of the multi-view reconstruction, we respectively predict the pose of the 3D faces in the multi-view [44], instead of only predicting the pose of one perspective to render 2D images.

4. Weakly Supervised Training

In order to alleviate the strong need for the labeled data, we design a weakly supervised method for training. First, we render the predicted 3D

face model back to 2D and compare the rendered image with the original image pixel by pixel. Then, the rendered 2D images are fed into the face parse network to generate rendered face masks. According to the consistency principle, the rendered face masks should be consistent with the original face masks. Therefore, the L2 distance is treated as a mask loss. Finally, the landmark loss and regularization loss are introduced to shape 3D face and suppress the generation of distorted faces.

4.1. Photo Loss

Photo loss is often used in weakly supervised face reconstruction tasks [45, 12, 16, 17]. Distinct with the traditional methods, we impose a weight for each pixel according to the facial features. The weight map is learned by the face mask \mathcal{M} of the original image I . In order to enhance the robustness of the weight map, we dilate \mathcal{M} with 20 pixel as \mathcal{M}_d , as shown in Fig. 4. The dilated image is divided into three levels to be the weight map. In weight map, facial features are marked as 254, the rest of the facial area is marked as 128, and the background is marked as 32. The multi-view photo loss can be expressed as:

$$L_p = \frac{1}{\mathcal{V}} \sum_{v=1}^{\mathcal{V}} \frac{\sum_{i \in \mathcal{P}^v} \mathcal{M}_{di}^v \cdot \|I_i^v - I_i^{v'}\|_2}{\sum_{i \in \mathcal{P}^v} \mathcal{M}_{di}^v}, \quad (2)$$

where \mathcal{V} is the number of the reconstructed views. \mathcal{V} is 3 in the proposed model. \mathcal{P}^v is the area where the rendered image $I^{v'}$ and the original image I^v intersect in the current view. i denotes pixel index, and $\|\cdot\|_2$ denotes the L2 norm.

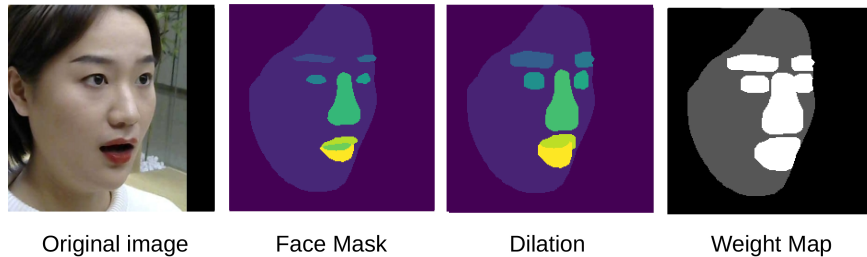


Figure 4: Weight Map

4.2. Mask Loss

Photo loss focuses on the pixel difference between two pictures. It is difficult to constrain the size of the facial feature area in the two pictures. For example, the nose color is very similar to that of the cheeks, thereby leading to difficulties for the photo loss to notice the boundary line between them. For this reason, we introduce mask loss to narrow the facial features of the input image and the rendered image. The division and labeling of the facial features are shown in Fig. 2. According to BiSeNet [37] we adopt cross entropy to calculate the mask loss L_m :

$$L_m = - \frac{1}{N_p \mathcal{V}} \sum_{v=1}^V \sum_{p=1}^{N_p} (y_p \log(\hat{y}_p) + (1 - y_p) \log(1 - \hat{y}_p)), \quad (3)$$

where N_p is number of pixels in face mask. \hat{y}_p donates the category prediction of pixels in face mask and y_p is the label.

4.3. Landmark Loss

We also adopt 2D landmarks and 3D landmarks for weakly supervised training. We use 3D face alignment method [46] to generate 68 landmarks

$\{l_n\}$ as the ground-truth. Then the corresponding points in the predicted 3D face point cloud are projected to 2D as predicted 2D landmarks $\{l'_n\}$. Then the multi-view 2D landmark loss can be calculated:

$$L_{l.2d} = \frac{1}{NV} \sum_{v=1}^V \sum_{n=1}^N \omega_n \left\| l_n^v - l'_n \right\|_2, \quad (4)$$

where ω_n is the weight for each landmark. We set the weight to 20 only for the nose and inner mouth landmarks, and to 1 otherwise.

2D landmarks are still insufficient for the reconstruction of 3D face shapes. In order to obtain better reconstruction effect, we select 101 3D landmarks $\{q'_n\}$ to impose a weak constraint on the shape of the 3D face. According to the 3DMM index, 101 predicted landmarks $\{q_n\}$ can be found. Then, we select 7 points $\{a'_n\}$ and $\{a_n\}$ in $\{q'_n\}$ and $\{q_n\}$ respectively as alignment points to calculate the alignment parameters of $\{q'_n\}$ and $\{q_n\}$. The alignment parameters include: scale \mathbf{s} , rotation \mathbf{R} and translation \mathbf{t} . These parameters can be obtained by the following optimization equation [47]:

$$Optim(\mathbf{s}, \mathbf{R}, \mathbf{t}) = \min_{\mathbf{s}, \mathbf{R}, \mathbf{t}} \sum_i \left\| \mathbf{a}'_i - \mathbf{s} (\mathbf{R} \cdot \mathbf{a}_i + \mathbf{t}) \right\|_2. \quad (5)$$

After the optimal \mathbf{s} , \mathbf{R} and \mathbf{t} are obtained, the predicted 101 landmarks $\{q_n\}$ can be converted to the space of $\{q'_n\}$ as $\{q_{nt}\} = \mathbf{s} (\mathbf{R} \cdot \mathbf{q}_n + \mathbf{t})$.

Then the multi-view 3D landmark loss can be calculated:

$$L_{l.3d} = \frac{1}{N} \sum_{n=1}^N \left\| q_{nt} - q'_n \right\|_2. \quad (6)$$

In summary, the landmark loss can be expressed as:

$$L_l = \omega_{2d} L_{l.2d} + \omega_{3d} L_{l.3d}, \quad (7)$$

where ω_{2d} and ω_{3d} represent respectively the weight of 2D landmark loss and 3D landmark loss. In this work, we set them to 0.02 and 1 as tuned empirically.

4.4. Regularization Loss

To suppress the generation of distorted faces, we add the regularization loss which is commonly-used in face reconstruction task [45, 12, 16, 17]:

$$L_{reg} = \omega_{\alpha} \|\boldsymbol{\alpha}\|^2 + \omega_{\beta} \|\boldsymbol{\beta}\|^2 + \omega_{\gamma} \|\boldsymbol{\gamma}\|^2, \quad (8)$$

where $\boldsymbol{\alpha}$, $\boldsymbol{\beta}$, and $\boldsymbol{\gamma}$ are 3DMM parameter vectors that the network predicted. ω_{α} , ω_{β} and ω_{γ} are the weights for 3DMM parameter vectors. Following Deep3DFace [16], we set them to 1, 0.8 and 0.017 with fine tuning.

4.5. Overall Loss

The overall loss required by our end-to-end net for weakly supervised training can be represented as:

$$L_{all} = \omega_p L_p + \omega_m L_m + \omega_l L_l + \omega_{reg} L_{reg},$$

where ω_p , ω_m , ω_l , ω_{reg} are the weights for photo loss, mask loss, landmark loss and regularization loss. Following Deep3DFace, we set $\omega_{reg} = 3.0 \times 10^{-4}$. Since ω_{2d} and ω_{3d} have been determined, we adjust other parameters as $\omega_l = 1$, $\omega_p = 4$ and $\omega_m = 3$ respectively.

Note that 3D landmarks is not a must for our method. For general weakly supervised methods, we do not incorporate $L_{l_{3d}}$ for comparison [16, 17]. Since semi-supervised methods HRN [36] adopts the entire 3D scans to attain training label, we add $L_{l_{3d}}$ for comparative analysis.

5. Experiment

5.1. Implementation Details

Dataset. Following BiSeNet [37], we adopt CelebAMask-HQ [48] to pre-train Face Parse Net. Furthermore, Pixel-Face [49] and Multi-PIE [50] are introduced to provide 3D landmarks label and multi-view faces. Pixel-Face contains 855 subjects ranging in age from 18 to 80 years old. Each subject has 7 or 23 samples of different expressions. Pixel-Face has 3D mesh file of each sample as ground-truth but not 3DMM parameters or angle of multi-view images. In the experiment, the training/test split was set to 0.8. For Multi-PIE, we leverage the version provided by TP-GAN [51], which will reduce a lot of data preprocessing work. This dataset contains about 140k multi-view images and does not provide 3D mesh and landmarks. We utilize the method of STNet [52] to detect and align faces. Then each input image is cropped and resized to 224×224 .

Network. Our network structure is shown in Fig. 1 and described in the methodology section. Based on the pre-trained BiSeNet [37] with frozen weights, the face parse network is located in the beginning and end of the network. We implement DF-MVR by pytorch [53]. It is trained on 2 NVIDIA RTX 3090 GPUs card with a batch size of 16 for 512 epochs. We adopt Adam as the gradient descent method. The initial learning rate is set to 0.0001 which decays with the cosine anneal schedule. The average inference time of DF-MVR is 244ms.

Evaluation Metric. Following the previous works, RMSE (mm) [35, 16, 17] is used to compute point-to-plane L2 distance between predict 3D scans and ground-truth 3D scans. Concretely, the front face area is cropped for metrics

calculation instead of using a complete BFM model [47, 16, 17]. Before calculating point-to-plane L2 distance, the predicted 3D scans need to be registered with ground-truth 3D scans. Also, we take the ICP registration method [54], the same as Deep3DFace [16].

5.2. Comparison to SOTAs

We compare our method with the existing weakly supervised MVRs on both Pixel-Face and Bosphorus datasets. More specifically, only the four methods with codes can be found in the literature related to multi-view weakly supervised 3D face reconstruction. MGCNet [17] takes multiple images for training, and then uses one single image for testing. We select the best results among the three images for display. Deep3DFace [16] does not release their source codes of its scoring network. Therefore, we use their codes to train/test on Pixel-Face to select the best results among the three images. Moreover, MVFR [18] necessitates scale_RT data, rendering it currently effective only for the Facescape dataset [55, 56]. HRN [36] does not release its training code, but it provides a pretrained model based on numerous data. To this end, we use its pretrained model and source code for multi-view face reconstruction. Given the scarcity of open sources for this task, we release our full codes (training & test) and pretrained model in GitHub².

Comparsion on Pixel-Face. The quantitative results of the comparison are shown in Table 1. Since MGCNet [17] and Deep3DFace [16] did not use 3D landmarks, to be fair, we also provide the results of our model without using 3D landmarks for comparison. As observed, Our model (without

²https://github.com/weiguangzhao/DF_MVR

Table 1: Comparison to SOTAs. † stands for the necessity to leverage 3D ground-truth (GT) data for semi-supervised training. HRN[†] utilizes the entire 3D ground-truth scan to attain both deformation and displacement maps. Ours[†] only takes a sparse set of 3D landmarks.

Method	Dataset	RMSE (mm) ↓
Deep3DFace [16]	Pixel-Face	1.6641
MGCNet [17]	Pixel-Face	1.8877
Ours	Pixel-Face	1.5770
HRN [†] [36]	Pixel-Face	1.4061
Ours [†]	Pixel-Face	1.4040
Deep3DFace [16]	Bosphorus	1.4777
MGCNet [17]	Bosphorus	1.4418
Ours	Bosphorus	1.3994

3D landmarks) shows 5.2% improvement compared to the existing methods. While HRN [36] adopts the complete 3D ground-truth scan to attain deformation map and displacement map, we only take very light annotation, 101 3D landmarks to constraint the face reconstruction. Ours[†] shows very competitive results with fewer 3D annotation, compared to HRN[†].

The visual comparison is shown in Fig. 5 given 3-view faces. It is evident that our predicted model is more accurate, especially in terms of facial depth estimation in the facial features.

Comparsion on Bosphorus. Since Pixel-Face dataset is collected based on Asian faces, the samples it contains are limited by regions. On the other hand, Pixel-Face dataset is only made under one lighting environment and three fixed camera angles. Taking into account the diversity, we adopt the

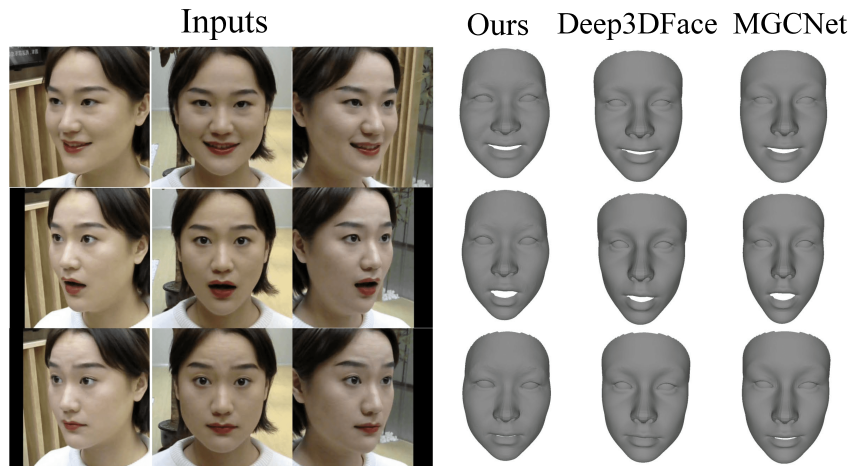


Figure 5: Qualitative Comparison on Pixel-Face

richer Multi-PIE dataset for training and Bosphorus dataset for testing. Both datasets contain faces across continents and are collected in various lighting environments and shooting angles. Because Multi-PIE does not provide 3D landmarks, we remove $L_{l_{3d}}$ to train DF-MVR for this part. The tradition delaunay algorithm is utilized to generate mesh files from point clouds for Bosphorus dataset. We set the left and right inputs to 45 degrees for comparison. More angle robustness experiments can be later seen in Table 4. The quantitative results of the comparison are shown in Table 1. Our model (without 3D landmarks) exhibits 3.0% improvement compared to the existing methods. The qualitative comparison is also provided in Fig. 6.

5.3. Single-view Reconstruction.

The single-view reconstruction method only requires one image to generate the 3D face. From the practical viewpoint, it is more flexible though it may be inferior to multi-view methods in terms of accuracy. Our method

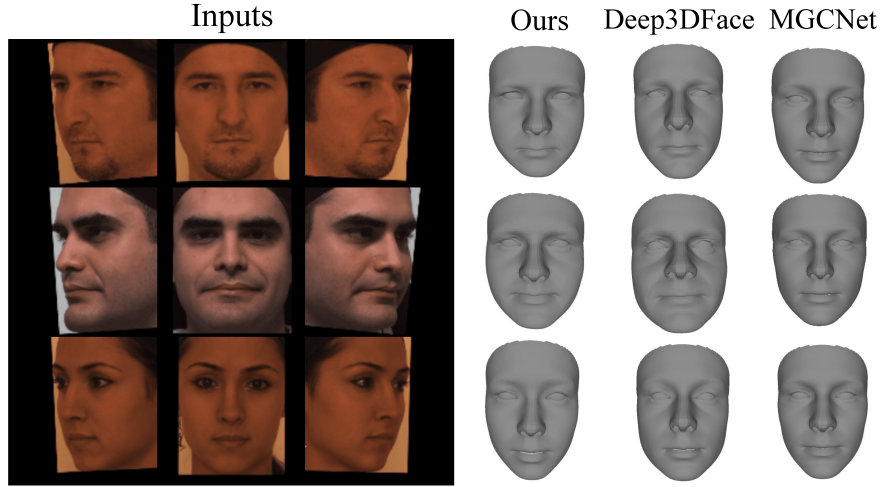


Figure 6: Qualitative Comparison on Bosphorus

can also be adapted in the single view scenario. More specifically, during the training process, we only change the input, without changing other parts. As shown in Fig. 7, the original input has been changed to four different forms, according to the probability: P'_a, P_1, P_f, P_r . The input of multi-view images still needs to be dominant to preserve accuracy, so we set its probability to $2/3$, and the other inputs equally distribute with the probability of $1/3$.

The parameterized results of the comparison are shown in Table 2. As observed, our proposed model also attains the superior performance. In the case of single image testing, our model is more effective than Deep3DFace and MGCNet.

5.4. Ablation Study

In order to verify the effectiveness of Tri-UNet and the mask mechanism we designed, we perform more ablation experiments as shown in Table 3. The mean and standard deviation of RMSE are again used as the evaluation met-

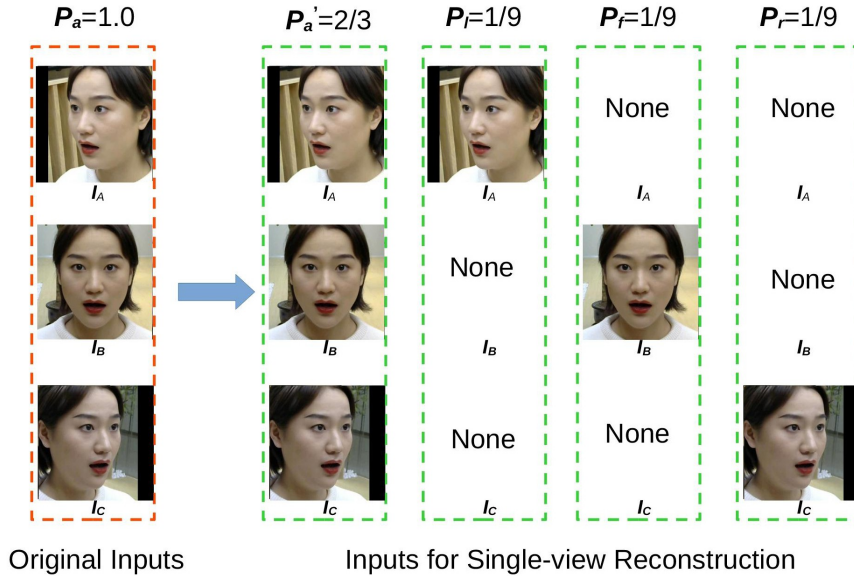


Figure 7: Inputs for Single-view Reconstruction. 'None' means a black image.

Table 2: Comparison of RMSE (mm)

Method	Dataset	RMSE (mm) ↓
Shang et al. [17]	Pixel-Face	1.8877
Deng et al. [16]	Pixel-Face	1.6641
Ours (single-view)	Pixel-Face	1.5437

ric. First, from v1, v2, v6, it can be found that the multi-view feature fusion network we designed is superior to traditional CNN and Unet in this task. Then, the results of v2 and v6 hint that the multi-layer feature interaction in the feature extraction stage is better than the direct concatenation of features at the end. To be fair, we set the number of layers of RedNet and ResNet to 50. Through the RMSE of v3 and v6, it is clear that RedNet performs better than ResNet in this task. For v4, we not only remove the mask loss but also

the face mask \mathbf{I}_A , \mathbf{I}_B and \mathbf{I}_C , which are concatenated to the original image. By comparing v5 and v6, we can see that the face mask mechanism promotes the network to generate a higher-precision model. Moreover, we verify the face mask and mask loss separately. Mask loss has a much smaller effect on the accuracy of the model than face mask. While the qualitative result of mask loss is positive for the adjustment of the model during training, we retain this part for reference. Finally, we remove $L_{lan.3d}$, which means that our model can be trained with only three multi-view images without any 3D label (as denoted as v5). The result also shows that our model is accurate and stable.

Table 3: Ablation Study

Ours	Backbone	/	Facemask	$L_{l.3d}$	RMSE (mm) ↓
v1	CNN	RedNet	Y	Y	1.5415
v2	Unet	RedNet	Y	Y	1.5207
v3	Tri-Unet	ResNet	Y	Y	1.5206
v4	Tri-Unet	RedNet	N	Y	1.4656
v5	Tri-Unet	RedNet	Y	N	1.5770
v6	Tri-Unet	RedNet	Y	Y	1.4040

5.5. Robustness Analysis

Multi-PIE and Bosphorus are collected by different cameras. DF-MVR uses Multi-PIE for training and achieves good test results on Bosphorus, which implies that our model has a certain robustness to camera device changes. Moreover, we further explore robustness of DF-MVR for shooting angles. We fix the \mathbf{I}_B and \mathbf{I}_C face angles while adjusting the \mathbf{I}_A face angle.

Table 4 and Fig. 8(a) show that our model consistently achieve the best results in different shooting angles, implying that our model exhibits the best robustness. Random means we choose the degree from 10° , 20° , 30° and 45° randomly. The light environment is also random in this experiment.

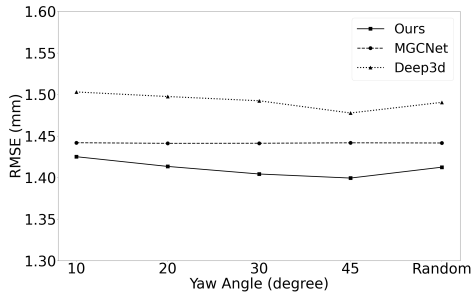
Table 4: Robustness Analysis on Bosphorus dataset.

Method	10°	20°	30°	45°	Random
Shang et al. [17]	1.4419	1.4412	1.4413	1.4418	1.4416
Deng et al. [16]	1.5030	1.4975	1.4924	1.4777	1.4905
Ours (v5)	1.4251	1.4134	1.4043	1.3994	1.4125

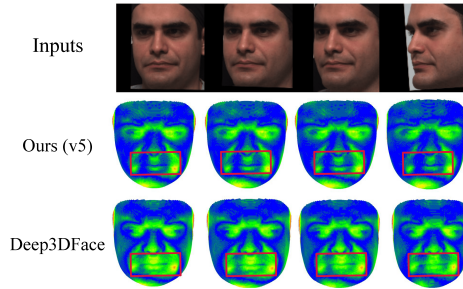
We also validate the angle robustness of our model visually. These results are plotted in Fig. 8(a). Detailed error maps are introduced to display the error for each facial area directly. Take the second sample of Fig. 8(b) for a typical example where we fix \mathbf{I}_B and \mathbf{I}_c while changing the face angle of \mathbf{I}_A from 10° to 45° . Obviously, the error maps generated from these angles do not change much. Furthermore, we provide the error maps of Deep3DFace [16] for comparison. At different angles, DF-MVR reconstructs the face with less error, especially in critical areas (e.g. eye, brow, nose and mouth).

6. Conclusion

In this paper, we design a novel end-to-end weakly supervised multi-view 3D face reconstruction network that exploits multi-view encoding to a single decoding framework with skip connections, able to extract, integrate, and compensate deep features with attention. In addition, we develop a multi-view face parse network to learn, identify, and emphasize the critical common



(a) Quantitative results on Bosphorus dataset.



(b) Reconstruction Error Maps. The errors are expressed from small to large in the following order: blue, green, yellow, red.

Figure 8: Robustness Analysis.

face area. Combining pixelwise photometric loss, mask loss, and landmark loss, we complete the weakly supervised training. Extensive experiments verify the effectiveness of our model.

7. Ethics Statement

In this paper, we presented visualizations of the results for Pixel-Face and Bosphorus dataset. Specifically, we have only showcased Pixel-Face facial information for a single individual, and this information has been obtained with the explicit consent of the individual and the Pixel Face dataset team, allowing for publication. Additionally, we presented Bosphorus facial information for three individuals, all of whom are included in the publicly disclosed roster of the Bosphorus dataset. Our approach leverages multi-view images to generate high-fidelity 3D facial models, meeting the demands of industries such as film, gaming, virtual characters, and more. Due to the strong privacy im-

plications associated with facial data, we suggest establishing detailed rules to regulate the use of facial reconstruction.

References

- [1] Hatef Otroushi Shahreza and Sébastien Marcel. Comprehensive vulnerability evaluation of face recognition systems to template inversion attacks via 3d face reconstruction. *IEEE Transactions on Pattern Analysis and Machine Intelligence (TPAMI)*, 2023.
- [2] Ruben Tolosana, Ruben Vera-Rodriguez, Julian Fierrez, Aythami Morales, and Javier Ortega-Garcia. Deepfakes and beyond: A survey of face manipulation and fake detection. *Information Fusion (IF)*, 64: 131–148, 2020.
- [3] Weiyi Kong, Zhisheng You, Shiyang Lyu, and Xuebin Lv. Multi-dimensional stereo face reconstruction for psychological assistant diagnosis in medical meta-universe. *Information Science (IS)*, page 119831, 2023.
- [4] Volker Blanz and Thomas Vetter. A morphable model for the synthesis of 3d faces. In *Proceedings of the ACM Siggraph (SIGGRAPH)*, pages 187–194, 1999.
- [5] Pengfei Dou and Ioannis A Kakadiaris. Multi-view 3d face reconstruction with deep recurrent neural networks. *Image and Vision Computing (IVC)*, 80:80–91, 2018.

- [6] Yao Feng, Fan Wu, Xiaohu Shao, Yanfeng Wang, and Xi Zhou. Joint 3d face reconstruction and dense alignment with position map regression network. In *Proceedings of the European conference on computer vision (ECCV)*, pages 534–551, 2018.
- [7] Yudong Guo, Jianfei Cai, Boyi Jiang, Jianmin Zheng, et al. Cnn-based real-time dense face reconstruction with inverse-rendered photo-realistic face images. *IEEE Transactions on Pattern Analysis and Machine Intelligence (TPAMI)*, 41(6):1294–1307, 2018.
- [8] Weiguang Zhao, Yuyao Yan, Chaolong Yang, Jianan Ye, Xi Yang, and Kaizhu Huang. Divide and conquer: 3d point cloud instance segmentation with point-wise binarization. In *Proceedings of the IEEE/CVF International Conference on Computer Vision (ICCV)*, pages 562–571, 2023.
- [9] Chenru Jiang, Kaizhu Huang, Junwei Wu, Xinheng Wang, Jimin Xiao, and Amir Hussain. Pointgs: Bridging and fusing geometric and semantic space for 3d point cloud analysis. *Information Fusion (IF)*, 91:316–326, 2023.
- [10] Ayush Tewari, Michael Zollhofer, Hyeongwoo Kim, Pablo Garrido, Florian Bernard, Patrick Perez, and Christian Theobalt. Mofa: Model-based deep convolutional face autoencoder for unsupervised monocular reconstruction. In *Proceedings of the IEEE/CVF International Conference on Computer Vision Workshop (ICCV)*, pages 1274–1283, 2017.
- [11] Anh Tuan Tran, Tal Hassner, Iacopo Masi, Eran Paz, Yuval Nirkin, and

- Gérard G Medioni. Extreme 3d face reconstruction: Seeing through occlusions. In *Proceedings of the IEEE/CVF Conference on Computer Vision and Pattern Recognition (CVPR)*, pages 3935–3944, 2018.
- [12] Ayush Tewari, Michael Zollhöfer, Pablo Garrido, Florian Bernard, Hyeonwoo Kim, Patrick Pérez, and Christian Theobalt. Self-supervised multi-level face model learning for monocular reconstruction at over 250 hz. In *Proceedings of the IEEE/CVF Conference on Computer Vision and Pattern Recognition (CVPR)*, pages 2549–2559, 2018.
- [13] Shubhajit Basak, Peter Corcoran, Rachel McDonnell, and Michael Schukat. 3d face-model reconstruction from a single image: A feature aggregation approach using hierarchical transformer with weak supervision. *Neural Networks (NN)*, 156:108–122, 2022.
- [14] Erroll Wood, Tadas Baltrušaitis, Charlie Hewitt, Matthew Johnson, Jingjing Shen, Nikola Milosavljević, Daniel Wilde, Stephan Garbin, Toby Sharp, Ivan Stojiljković, et al. 3d face reconstruction with dense landmarks. In *Proceedings of the European conference on computer vision (ECCV)*, pages 160–177, 2022.
- [15] Chunlu Li, Andreas Morel-Forster, Thomas Vetter, Bernhard Egger, and Adam Kortylewski. Robust model-based face reconstruction through weakly-supervised outlier segmentation. In *Proceedings of the IEEE/CVF Conference on Computer Vision and Pattern Recognition (CVPR)*, pages 372–381, 2023.
- [16] Yu Deng, Jiaolong Yang, Sicheng Xu, Dong Chen, Yunde Jia, and

- Xin Tong. Accurate 3d face reconstruction with weakly-supervised learning: From single image to image set. In *Proceedings of the IEEE/CVF Conference on Computer Vision and Pattern Recognition Workshop (CVPRW)*, 2019.
- [17] Jiaxiang Shang, Tianwei Shen, Shiwei Li, Lei Zhou, Mingmin Zhen, Tian Fang, and Long Quan. Self-supervised monocular 3d face reconstruction by occlusion-aware multi-view geometry consistency. In *Proceedings of the European conference on computer vision (ECCV)*, pages 53–70. Springer, 2020.
- [18] Yunze Xiao, Hao Zhu, Haotian Yang, Zhengyu Diao, Xiangju Lu, and Xun Cao. Detailed facial geometry recovery from multi-view images by learning an implicit function. In *Proceedings of the AAAI Conference on Artificial Intelligence (AAAI)*, 2022.
- [19] Duo Li, Jie Hu, Changhu Wang, Xiangtai Li, Qi She, Lei Zhu, Tong Zhang, and Qifeng Chen. Involution: Inverting the inherence of convolution for visual recognition. In *Proceedings of the IEEE/CVF Conference on Computer Vision and Pattern Recognition (CVPR)*, pages 12321–12330, 2021.
- [20] Paul Koppen, Zhen-Hua Feng, Josef Kittler, Muhammad Awais, William Christmas, Xiao-Jun Wu, and He-Feng Yin. Gaussian mixture 3d morphable face model. *Pattern Recognition (PR)*, 74:617–628, 2018.
- [21] Pascal Paysan, Reinhard Knothe, Brian Amberg, Sami Romdhani, and

- Thomas Vetter. A 3d face model for pose and illumination invariant face recognition. In *Proceedings of the IEEE International Conference on Advanced Video and Signal Based Surveillance (AVSS)*, pages 296–301, 2009.
- [22] James Booth, Anastasios Roussos, Allan Ponniah, David Dunaway, and Stefanos Zafeiriou. Large scale 3d morphable models. *International Journal of Computer Vision (IJCV)*, 126(2):233–254, 2018.
- [23] Michael J Jones and James M Rehg. Statistical color models with application to skin detection. *International Journal of Computer Vision (IJCV)*, 46:81–96, 2002.
- [24] Jiangke Lin, Yi Yuan, Tianjia Shao, and Kun Zhou. Towards high-fidelity 3d face reconstruction from in-the-wild images using graph convolutional networks. In *Proceedings of the IEEE/CVF Conference on Computer Vision and Pattern Recognition (CVPR)*, pages 5891–5900, 2020.
- [25] Dapeng Zhao and Yue Qi. Generative face parsing map guided 3d face reconstruction under occluded scenes. In *Proceedings of Advances in Computer Graphics: Computer Graphics International Conference (CGI)*, pages 252–263, 2021.
- [26] Xiangyu Zhu, Zhen Lei, Xiaoming Liu, Hailin Shi, and Stan Z Li. Face alignment across large poses: A 3d solution. In *Proceedings of the IEEE/CVF Conference on Computer Vision and Pattern Recognition (CVPR)*, pages 146–155, 2016.

- [27] Anh Tuan Tran, Tal Hassner, Iacopo Masi, and Gerard Medioni. Regressing robust and discriminative 3d morphable models with a very deep neural network. In *Proceedings of the IEEE/CVF Conference on Computer Vision and Pattern Recognition (CVPR)*, pages 5163–5172, 2017.
- [28] Yueying Kao, Bowen Pan, Miao Xu, Jiangjing Lyu, Xiangyu Zhu, Yuanzhang Chang, Xiaobo Li, and Zhen Lei. Towards 3d face reconstruction in perspective projection: Estimating 6dof face pose from monocular image. *IEEE Transactions on Image Processing (TIP)*, 2023.
- [29] Kaiming He, Xiangyu Zhang, Shaoqing Ren, and Jian Sun. Deep residual learning for image recognition. In *Proceedings of the IEEE/CVF Conference on Computer Vision and Pattern Recognition (CVPR)*, pages 770–778, 2016.
- [30] Pengfei Dou, Shishir K Shah, and Ioannis A Kakadiaris. End-to-end 3d face reconstruction with deep neural networks. In *Proceedings of the IEEE/CVF Conference on Computer Vision and Pattern Recognition (CVPR)*, pages 5908–5917, 2017.
- [31] Kyle Genova, Forrester Cole, Aaron Maschinot, Aaron Sarna, Daniel Vlasic, and William T Freeman. Unsupervised training for 3d morphable model regression. In *Proceedings of the IEEE/CVF Conference on Computer Vision and Pattern Recognition (CVPR)*, pages 8377–8386, 2018.
- [32] Soumyadip Sengupta, Angjoo Kanazawa, Carlos D Castillo, and David W Jacobs. Sfsnet: Learning shape, reflectance and illuminance

- of faces in the wild'. In *Proceedings of the IEEE/CVF Conference on Computer Vision and Pattern Recognition (CVPR)*, pages 6296–6305, 2018.
- [33] Ziqian Bai, Zhaopeng Cui, Jamal Ahmed Rahim, Xiaoming Liu, and Ping Tan. Deep facial non-rigid multi-view stereo. In *Proceedings of the IEEE/CVF Conference on Computer Vision and Pattern Recognition (CVPR)*, pages 5850–5860, 2020.
- [34] Eduard Ramon, Janna Escur, and Xavier Giró-i Nieto. Multi-view 3d face reconstruction in the wild using siamese networks. In *Proceedings of the IEEE/CVF Conference on Computer Vision and Pattern Recognition Workshop (CVPRW)*, 2019.
- [35] Fanzi Wu, Linchao Bao, Yajing Chen, Yonggen Ling, Yibing Song, Songnan Li, King Ng Ngan, and Wei Liu. Mvf-net: Multi-view 3d face morphable model regression. In *Proceedings of the IEEE/CVF Conference on Computer Vision and Pattern Recognition (CVPR)*, pages 959–968, 2019.
- [36] Biwen Lei, Jianqiang Ren, Mengyang Feng, Miaomiao Cui, and Xuan-song Xie. A hierarchical representation network for accurate and detailed face reconstruction from in-the-wild images. In *Proceedings of the IEEE/CVF Conference on Computer Vision and Pattern Recognition (CVPR)*, pages 394–403, 2023.
- [37] Changqian Yu, Jingbo Wang, Chao Peng, Changxin Gao, Gang Yu, and Nong Sang. Bisenet: Bilateral segmentation network for real-time

- semantic segmentation. In *Proceedings of the European conference on computer vision (ECCV)*, pages 325–341, 2018.
- [38] Ozan Oktay, Jo Schlemper, Loic Le Folgoc, Matthew Lee, Mattias Heinrich, Kazunari Misawa, Kensaku Mori, Steven McDonagh, Nils Y Hammerla, Bernhard Kainz, et al. Attention u-net: Learning where to look for the pancreas. In *Proceedings of the Medical Imaging with Deep Learning (MIDL)*, 2018.
- [39] Dzmitry Bahdanau, Kyung Hyun Cho, and Yoshua Bengio. Neural machine translation by jointly learning to align and translate. In *Proceedings of the International Conference on Learning Representations (ICLR)*, 2015.
- [40] Zihan Ye, Fan Lyu, Linyan Li, Yu Sun, Qiming Fu, and Fuyuan Hu. Un-supervised object transfiguration with attention. *Cognitive Computation (CC)*, 11:869–878, 2019.
- [41] Amit Chougule, Agneya Bhardwaj, Vinay Chamola, and Pratik Narang. Agd-net: Attention-guided dense inception u-net for single-image dehazing. *Cognitive Computation*, pages 1–14, 2023.
- [42] Chen Cao, Yanlin Weng, Shun Zhou, Yiying Tong, and Kun Zhou. Face-warehouse: A 3d facial expression database for visual computing. *IEEE Transactions on Visualization and Computer Graphics (TVCG)*, 20(3): 413–425, 2013.
- [43] Nikhila Ravi, Jeremy Reizenstein, David Novotny, Taylor Gordon, Wan-

- Yen Lo, Justin Johnson, and Georgia Gkioxari. Accelerating 3d deep learning with pytorch3d. *ArXiv Preprint ArXiv:2007.08501*, 2020.
- [44] Jian Dai, Zhenwen Ren, Yunzhi Luo, Hong Song, and Jian Yang. Tensorized anchor graph learning for large-scale multi-view clustering. *Cognitive Computation (CC)*, pages 1–12, 2023.
- [45] Justus Thies, Michael Zollhofer, Marc Stamminger, Christian Theobalt, and Matthias Nießner. Face2face: Real-time face capture and reenactment of rgb videos. In *Proceedings of the IEEE/CVF Conference on Computer Vision and Pattern Recognition (CVPR)*, pages 2387–2395, 2016.
- [46] Adrian Bulat and Georgios Tzimiropoulos. How far are we from solving the 2d & 3d face alignment problem? In *Proceedings of the IEEE/CVF International Conference on Computer Vision (ICCV)*, pages 1021–1030, 2017.
- [47] Soubhik Sanyal, Timo Bolkart, Haiwen Feng, and Michael J Black. Learning to regress 3d face shape and expression from an image without 3d supervision. In *Proceedings of the IEEE/CVF Conference on Computer Vision and Pattern Recognition (CVPR)*, pages 7763–7772, 2019.
- [48] Cheng-Han Lee, Ziwei Liu, Lingyun Wu, and Ping Luo. Maskgan: Towards diverse and interactive facial image manipulation. In *Proceedings of the IEEE/CVF Conference on Computer Vision and Pattern Recognition (CVPR)*, 2020.

- [49] Jiangjing Lyu, Xiaobo Li, Xiangyu Zhu, and Cheng Cheng. Pixel-face: A large-scale, high-resolution benchmark for 3d face reconstruction. *ArXiv Preprint ArXiv:2008.12444*, 2020.
- [50] Ralph Gross, I. Matthews, Jeffrey F. Cohn, Takeo Kanade, and Simon Baker. Multi-pie. In *Proceedings of the IEEE International Conference on Automatic Face & Gesture Recognition (FG)*, pages 1–8, 2008.
- [51] Rui Huang, Shu Zhang, Tianyu Li, and Ran He. Beyond face rotation: Global and local perception gan for photorealistic and identity preserving frontal view synthesis. In *Proceedings of the IEEE/CVF International Conference on Computer Vision (ICCV)*, pages 2458–2467, 2017.
- [52] Dong Chen, Gang Hua, Fang Wen, and Jian Sun. Supervised transformer network for efficient face detection. In *Proceedings of the European conference on computer vision (ECCV)*, pages 122–138, 2016.
- [53] Adam Paszke, Sam Gross, Francisco Massa, Adam Lerer, James Bradbury, Gregory Chanan, Trevor Killeen, Zeming Lin, Natalia Gimelshein, Luca Antiga, Alban Desmaison, Andreas Köpf, Edward Yang, Zach DeVito, Martin Raison, Alykhan Tejani, Sasank Chilamkurthy, Benoit Steiner, Lu Fang, Junjie Bai, and Soumith Chintala. Pytorch: An imperative style, high-performance deep learning library. In *Proceedings of the Advances in Neural Information Processing Systems (NeurIPS)*, 2019.
- [54] Tianye Li, Timo Bolkart, Michael. J. Black, Hao Li, and Javier Romero.

Learning a model of facial shape and expression from 4D scans. *ACM Transactions on Graphics (TOG)*, 36(6), 2017.

[55] Haotian Yang, Hao Zhu, Yanru Wang, Mingkai Huang, Qiu Shen, Ruigang Yang, and Xun Cao. Facescape: a large-scale high quality 3d face dataset and detailed riggable 3d face prediction. In *Proceedings of the IEEE/CVF Conference on Computer Vision and Pattern Recognition (CVPR)*, 2020.

[56] Hao Zhu, Haotian Yang, Longwei Guo, Yidi Zhang, Yanru Wang, Mingkai Huang, Menghua Wu, Qiu Shen, Ruigang Yang, and Xun Cao. Facescape: 3d facial dataset and benchmark for single-view 3d face reconstruction. *IEEE Transactions on Pattern Analysis and Machine Intelligence (TPAMI)*, 2023.